J Electr Eng Technol.2015; 10(3): 958-964
http://dx.doi.org/10.5370/JEET.2015.10.3.958

ISSN(Print) 1975-0102
ISSN(Online) 2093-7423

Dynamic Analysis of Double Excited 3-DOF Motor Modeling Using Equivalent Magnetic Circuit

Se-Hyun Rhyu*, Hye-Ung Shin, Min-Soo Kim** and Byung-Il Kwon†**

Abstract – This paper implements a model of a double excited three-degree-of-freedom motor (3-DOF) coupled with a PI current controller for position control. The rotational trends of the rotor according to the applied steps are identified using a motion equation. The simulation model is a complete electrical and mechanical model of a 3-DOF motor, which mainly consists of mechanical torque equations, a nonlinear equivalent magnetic circuit, and a PI current controller. This machine is tested using the manufactured control board using the same conditions as in the simulation, where the experimental results also verify the accuracy of the simulation results.

Keywords: 3-DOF motor, Dynamic analysis, Equivalent magnetic circuit, PI control

1. Introduction

Multiple degree of freedom motors have been a topic of interest due to their wide application in industry, such as for helicopters, boat propellers, robots, and so on [1-5]. The 3-DOF machine studied in this paper does not contain any permanent magnets and only field excitation is used, which reduces both the size and cost of the machine [6-7]. The position and torque control of the 3-DOF motor are important factors because industrial robots require exact position movement with strong force. Typically, the 3-D finite element method (FEM) is used to analyze the characteristics of a 3-DOF motor; however, the modeling and simulation of 3-D FEM consume a great deal of time and require a large number of calculation devices. The nonlinear equivalent magnetic circuits of a 3-DOF machine have been studied to reduce the simulation time, and have similar results to those obtained through a 3-D FEM analysis [8-10]. In addition, the simulation result of a dynamic characteristic analysis can identify the rotational trend of the rotor [11].

This paper presents the equivalent circuit of a 3-DOF motor that implements the mechanical torque equation, a nonlinear magnetic equivalent circuit, and a PI current controller as a part of the position control of the motor using Matlab / Simulink. The control board of the 3-DOF motor is designed according to each phase of the stator and rotor. Moreover, the experimental results validate the simulation results obtained by this simulation model.

† Corresponding Author: Dept. of Electrical and Electronic Engineering, Hanyang University, Korea. (bikwon@hanyang.ac.kr)
* Dept. of Intelligent Mechatronics Research Center, Korea Electronics Technology Institute, Korea. (rhyush@keti.re.kr)
** Dept. of Electrical and Electronic System Engineering, Hanyang University, Korea. (hyeung123@naver.com, msook@hanyang.ac.kr.)
Received: April 21, 2014; Accepted: November 18, 2014

2. Structure and Principle of Double Excited 3-DOF Motor

2.1 Structure of 3-DOF motor

The 3-DOF machine has three stator phases (U, V, and W) and ten rotor phases, with five each for rolling and pitching (A, B, C, D, and E). A universal bearing is used to hold the shaft, and slip rings are used to supply the rotor windings. Fig. 1 shows the structure of a 3-DOF motor [7].

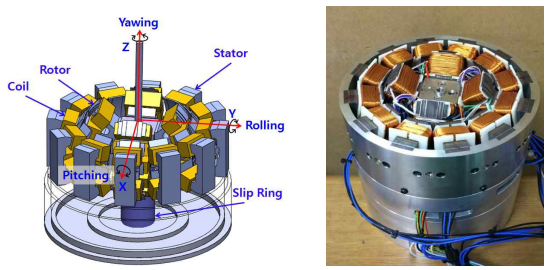

(a) (b)

Fig. 1. Double excited 3-DOF motor: (a) drawing model, and (b) manufactured model [7].

Table 1. The specification of double excited 3-DOF motor

			Unit	Value
Average Torque	Roll, pitch		Nm	0.14
	Yaw		Nm	0.739
Rotation Range	Roll, pitch		degree	±30
	Yaw		degree	±360
Rotor	Outer diameter		mm	104
	Input current		A	2.5
	Coil	Diameter	mm	0.8
		Turns	-	65
Stator	Outer diameter		mm	166
	Input current		A	2.5
	Coil	Diameter	mm	0.8
		Turns	-	85

The rolling and pitching can rotate from 5 degrees to 30 degrees with resolution of 5 degrees, while the yawing can rotate from 15 to 360 degrees with resolution of 15 degrees. Fig. 1 (a) shows the drawing model, while Fig. 1 (b) shows the manufactured model of the 3-DOF motor. Moreover, S-18 non-oriented electrical steel sheets are used for the stator and rotor cores. Table 1 shows the basic specification of the double excited 3-DOF motor in which the input DC current is 2.5 Amperes for operating a double excited 3-DOF motor.

2.2 Principle of 3-DOF motor

The single step operation of the machine is represented in Fig. 2. Initially, phases B and D from the rotor and phase U from the stator are excited to establish the flux path as shown in Fig. 2 (a). This excitation configuration gives the rotor position as zero degrees in the rolling direction. During the next step, phase D is unenergized while phase C is energized, which establishes the unbalanced flux path as shown in Fig. 2 (b). Due to this unbalanced flux path, the rotor rotates 10 degrees, and the flux path is now balanced as shown in Fig. 2(c). This rotation is generated due to the reluctance torque, which forces the rotor and stator teeth to be aligned for minimum reluctance. The rolling pole and pitching pole can rotate 30 degrees.

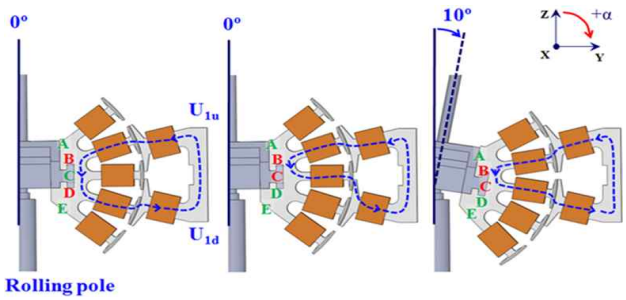

(a) (b) (c)

Fig. 2 Principle of rolling motion: (a) excited B and D, (b) excited B and C (unbalanced), and (c) excited B and C (balanced).

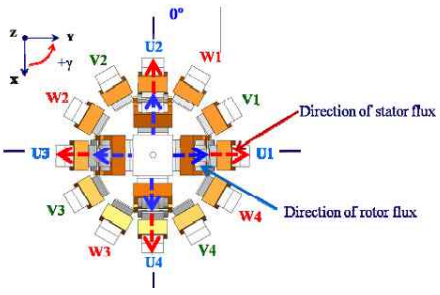

(a)

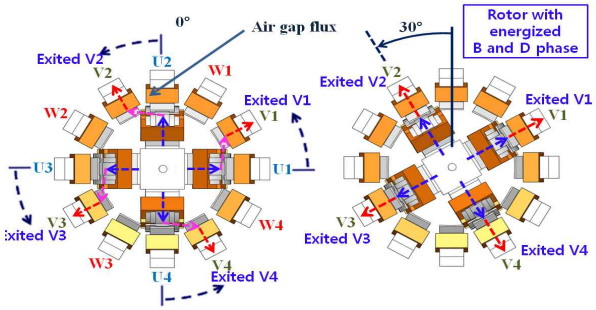

(b) (c)

Fig. 3. Principle of yawing: (a) phase U excited, (b) phase V excited (unbalanced), and (c) phase V excited (balanced).

Fig. 3 demonstrates the principle of operation of the yawing pole of the 3-DOF motor. Fig. 3 (a) shows zero degree alignment when phases B and D of the rotor and phase U of the stator are energized. Phase V of the stator is excited as shown in Fig. 3 (b), and the rotor rotates to minimize the magnetic reluctance, so the reluctance torque is generated. Fig. 3 (c) shows a rotor rotation of 30 degrees due to this reluctance torque. Slip rings are provided to energize the rotor phases; otherwise, the direct wire connections at the rotor phases would exert force on the rotor and the torque would be disturbed. Furthermore, the direct connection without the slip rings at the rotor phases would impede the 360 degree rotation of the rotor shaft.

3. Dynamic Characteristic Analysis

3.1 Nonlinear equivalent magnetic circuit

Machine modeling with a nonlinear equivalent magnet circuit is shown in Fig. 4 [8]. The yawing and rolling poles are shown in Fig. 4(a) and Fig. 4(b), respectively. The core saturation, leakage flux, and fringing effects are taken into consideration while developing the nonlinear equivalent magnetic circuit. An iterative method using the B/H curve is adopted for core saturation consideration.

Fig. 5 presents the air gap of the rolling direction. Fig. 5(a) shows the normal air gap flux when the excited teeth areas of the rotor and stator overlap each other. Fig. 5(b) shows the path of the fringing effect where it passes through the corner of the rotor teeth shoe, although it links

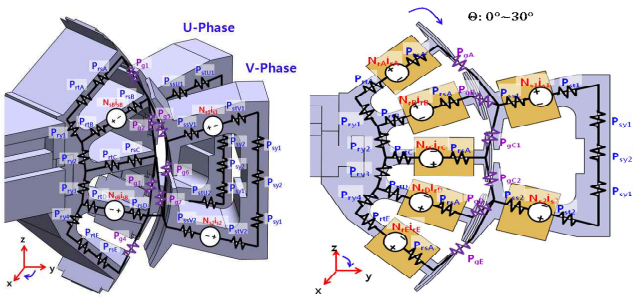

(a) (b)

Fig. 4. Equivalent magnetic circuit of double excited 3-DOF motor: (a) Yawing direction (b) Rolling, Pitching direction.

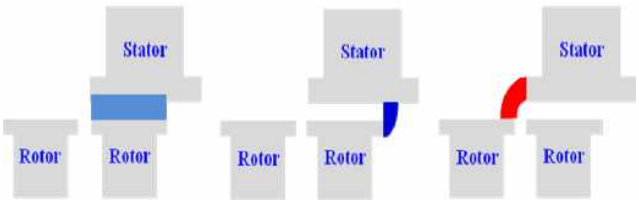

Fig. 5. Airgap of double excited 3-DOF actuator: (a) normal flux, (b) fringing effect, and (c) leakage flux.

the excited teeth. Fig. 5(c) depicts the shape of the leakage flux that flows from the excited stator teeth to the non-excited rotor teeth. The permeance values that are caused by the normal flux, fringing effect, and leakage are calculated by Eqs. (1), (2), and (3), respectively. These three equations consider different kinds of rotor positions with respect to the stator.

$$P_{g1} = \frac{\mu_0 A_g}{g} \tag{1}$$

$$P_{g2} = \frac{2\mu_0 L}{\pi} \ln |x| \tag{2}$$

$$P_{g3} = \frac{2\mu_0 L}{\pi} \ln \left|1 + \frac{\pi x}{2g}\right| \tag{3}$$

where Ag, L, g, and x are the cross area of the air gap, stack length, air gap length, and the average length of the leakage flux path in the air gap, respectively. The node matrix method uses the flux source to calculate the magnetic potential of each node, so every MMF source should be changed to a flux source. Fig. 6 illustrates the transformation from an MMF source to a flux source in the equivalent magnetic circuit.

This transformation from an MMF source to a flux source is defined by Eq. (4):

$$\left.\begin{aligned} F_{m0}(i) &= Ni \\ \Phi_{0n}(i) &= F_{m0}(i) P(i) \end{aligned}\right\} \tag{4}$$

where, F_n, $F_{m0}(i)$, $\Phi_{0n}(i)$, $\phi(i)$, N, i and $P(i)$ are the magnetic potential of the nodes, MMF source, flux source, flux of each node, number of winding turns, related current source, and permeance of each node, respectively.

A flow chart for the nonlinear equivalent magnetic

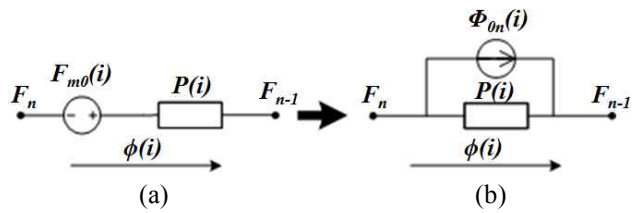

Fig. 6. Change to flux source from magnetomotive force source (a) MMF source (b) flux source.

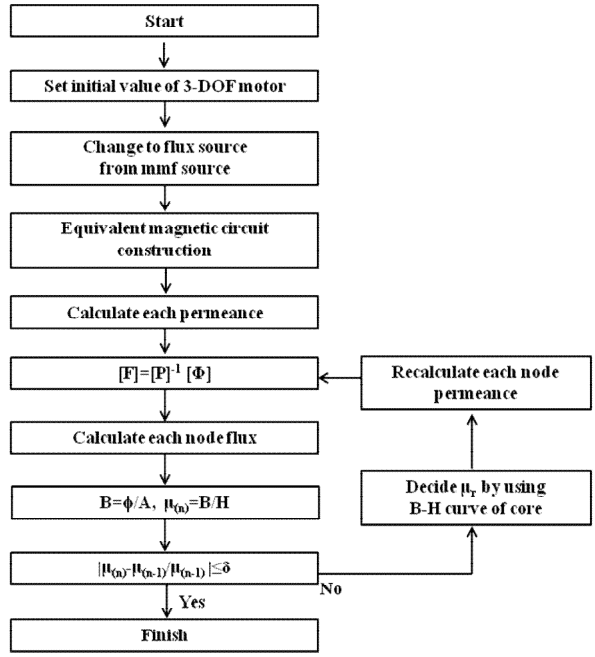

Fig. 7. Nonlinear magnetic analysis flowchart.

circuit calculations is given in Fig. 7. The reluctance torque and inductance, which are used in the voltage equation, are obtained using the flow chart for the nonlinear magnetic circuit.

3.2 Simulation modeling of 3-DOF motor

The model for the dynamic analysis of the system requires both mechanical and electrical modeling of the machine. The seven phases of the rotor and the stator as shown in Fig. 8 (Rotor: A_r, B_r, C_r, D_r, E_r Stator: U_1, U_2) provide sufficient information to develop the electrical model of the machine.

Eq. (5) represents the electrical system of this model in matrix form.

$$V_{U_1U_2ABCDE} = R_{U_1U_2ABCDE} i_{U_1U_2ABCDE} + \frac{d\lambda_{U_1U_2ABCDE}}{dt} \tag{5}$$

where $\boldsymbol{V}$ is the voltage, $\boldsymbol{R}$ is the resistance, $\boldsymbol{i}$ is the current,

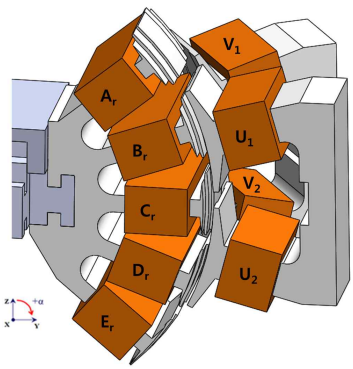

Fig. 8 Basic 3-DOF modeling model.

and λ represents the flux linkage of the machine.

Eq. (6) gives the voltage vector for the seven phases of the machine.

$$V_{U_1U_2ABCDE} = [V_{U_1} V_{U_2} V_A V_B V_C V_D V_E]^T \tag{6}$$

Eq. (7) gives the resistance and current matrix for this system. The variables in Eq. (6) and Eq. (7) depend upon the position of the rotor because different phases are energized at different positions.

$$R_{U_1U_2ABCDE} i_{U_1U_2ABCDE} = \begin{bmatrix} R_{U_1} & 0 & 0 & 0 & 0 & 0 & 0 \\ 0 & R_{U_2} & 0 & 0 & 0 & 0 & 0 \\ 0 & 0 & R_A & 0 & 0 & 0 & 0 \\ 0 & 0 & 0 & R_B & 0 & 0 & 0 \\ 0 & 0 & 0 & 0 & R_C & 0 & 0 \\ 0 & 0 & 0 & 0 & 0 & R_D & 0 \\ 0 & 0 & 0 & 0 & 0 & 0 & R_E \end{bmatrix} \begin{bmatrix} i_{U_1} \\ i_{U_2} \\ i_A \\ i_B \\ i_C \\ i_D \\ i_E \end{bmatrix} \tag{7}$$

The flux linkages in terms of the phase currents and inductances are presented in Eq. (8), where the inductances are combinations of the self and mutual inductances. Also, these variables can change their position in the matrix according to the rotor position. Therefore, lookup tables should be provided for each discrete position of the rotor.

Where, L_{U1U1} represents the self inductance of phase U, and L_{U1U2} shows the mutual component of the phase U inductance.

$$\lambda_{U_1U_2ABCDE} = \begin{bmatrix} L_{U_1U_1} & L_{U_1U_2} & L_{U_1A} & L_{U_1B} & L_{U_1C} & L_{U_1D} & L_{U_1E} \\ L_{U_2U_1} & L_{U_2U_2} & L_{U_2A} & L_{U_2B} & L_{U_2C} & L_{U_2D} & L_{U_2E} \\ L_{AU_1} & L_{AU_2} & L_{AA} & L_{AB} & L_{AC} & L_{AD} & L_{AE} \\ L_{BU_1} & L_{BU_2} & L_{BA} & L_{BB} & L_{BC} & L_{BD} & L_{BE} \\ L_{CU_1} & L_{CU_2} & L_{CA} & L_{CB} & L_{CC} & L_{CD} & L_{CE} \\ L_{DU_1} & L_{DU_2} & L_{DA} & L_{DB} & L_{DC} & L_{DD} & L_{DE} \\ L_{EU_1} & L_{EU_2} & L_{EA} & L_{EB} & L_{EC} & L_{ED} & L_{EE} \end{bmatrix} \begin{bmatrix} i_{U_1} \\ i_{U_2} \\ i_A \\ i_B \\ i_C \\ i_D \\ i_E \end{bmatrix} \tag{8}$$

Eq. (9) represents the voltage variations for the one-step operation of the rolling pole. The formulation of the pitching pole is exactly like that of the rolling pole, so only the rolling pole modeling is presented here. The rolling pole can be represented by a 4x4 matrix because four phases are excited at a time. The yawing pole is also formulated in the same way.

Also, Eq. (10) represents the mechanical dynamic equation of the system. It gives the relationship between the torque and position variation with respect to time.

$$\begin{aligned} i_{U_1}(t) &= \frac{1}{L_{U_1U_1}} \int_0^t [V_{U_1}(t) - R_{U_1} i_{U_1}(t)] dt \\ &\quad - \frac{1}{L_{U1U1}} (L_{U_1U_2} i_{U_2}(t) + L_{U_1B} i_B(t) + L_{U_1C} i_C(t)) \\ i_{U_2}(t) &= \frac{1}{L_{U_2U_2}} \int_0^t [V_{U_2}(t) - R_{U_2} i_{U_2}(t)] dt \\ &\quad - \frac{1}{L_{U_2U_2}} (L_{U_2U_1} i_{U_1}(t) + L_{U_2B} i_B(t) + L_{U_2C} i_C(t)) \\ i_B(t) &= \frac{1}{L_{BB}} \int_0^t [V_B(t) - R_B i_B(t)] dt \\ &\quad - \frac{1}{L_{BB}} (L_{BU_1} i_{U_1}(t) + L_{BU_2} i_{U_2}(t) + L_{BC} i_C(t)) \\ i_C(t) &= \frac{1}{L_{CC}} \int_0^t [V_C(t) - R_C i_C(t)] dt \\ &\quad - \frac{1}{L_{CC}} (L_{CU_1} i_{U_1}(t) + L_{CU_2} i_{U_2}(t) + L_{CB} i_B(t)) \end{aligned} \tag{9}$$

$$T_e = J \frac{d^2\theta}{dt^2} + B \frac{d\theta}{dt} + T_L \tag{10}$$

where the motion equation presents the variation of the position according to the time. J is the inertia moment, B is the friction coefficient, and T_L is the load. The load torque in this equation is ignored because the experiment is performed without a load. Eq. (11) is a simplified version of Eq. (10) in terms of the position angle.

$$\theta = \frac{1}{J} \int_0^t \left[\int_0^t T_e dt - B\theta \right] dt \tag{11}$$

Fig. 9 shows the complete control system diagram of the machine. For each step operation, the four phases require an independent PI controller. The PWM switching frequency is 15 kHz.

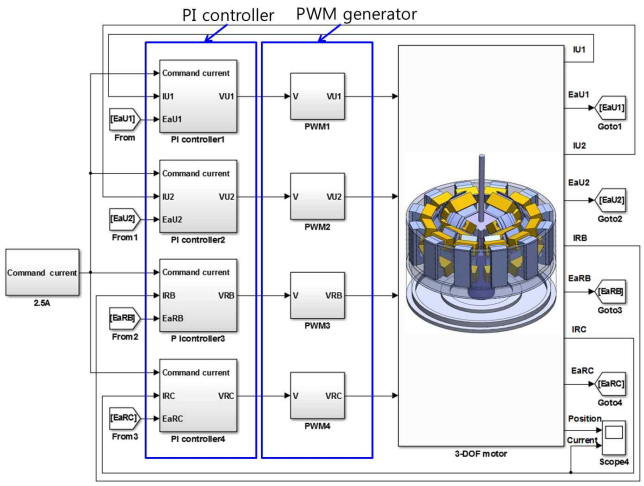

Fig. 9. Control interlock block diagram of double excited 3-DOF motor.

4. Simulation and Experiment

Fig. 10 shows the drive circuit for the rotor and stator phases of the machine. Fig. 10(a) presents the drive circuit of the stator, and Fig. 10(b) presents that of the rotor. U_1 represents the upper stator coil, whereas U_2 represents the lower stator coil. A DC supply of 2.5 Volts is applied to energize the phases.

The experimental setup is shown in Fig. 11. The experiment conditions are the same as those in the simulation. Four phases are energized at a time for one step movement, as explained previously. The feedback current is obtained using a current sensor, and then a PI controller is used to stabilize the current very quickly.

Fig. 12 shows 2 seconds of operation of the 3-DOF machine. The simulation and experimental results are provided when the PI current control is applied. Graphs are provided for the current versus time. Each current follows the command very well. The simulation results are similar to the experiment results.

Fig. 13 compares the results of the simulation and experiment as the rotor position of the machine with respect to time, where the experimental results validate the simulation results. There is only a slight difference in the results, which is due to the wire tensions that are applied to the rotor, even though the wire tensions are reduced by the slip ring. Fig. 13(c) has wire tension, which is more significant at 30 degrees than for the other steps. There is almost no wire tension applied to the rolling and pitching poles. However, the yawing pole has greater vibration of the rotor position than the other steps/poles.

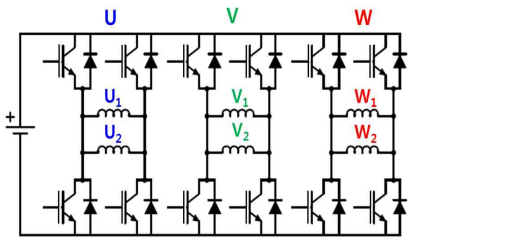

(a)

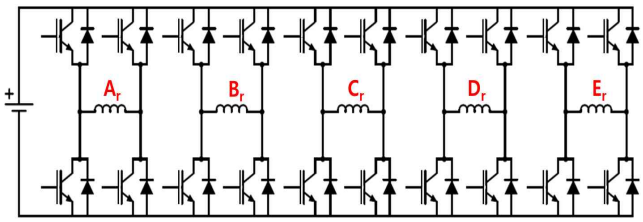

(b)

Fig. 10. Circuits of double excited 3-DOF motor: (a) Stator circuit; (b) Rotor circuit (Rolling pole).

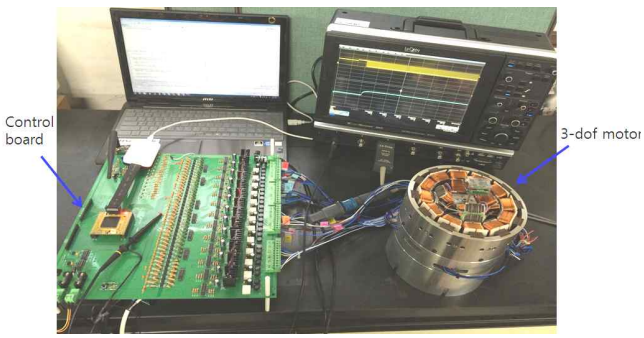

Fig. 11. PI current control experiment of double excited 3-DOF motor.

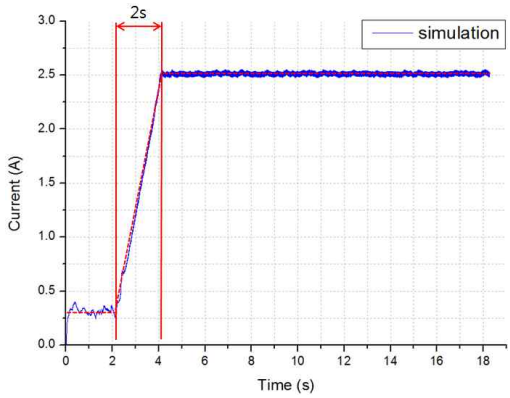

(a)

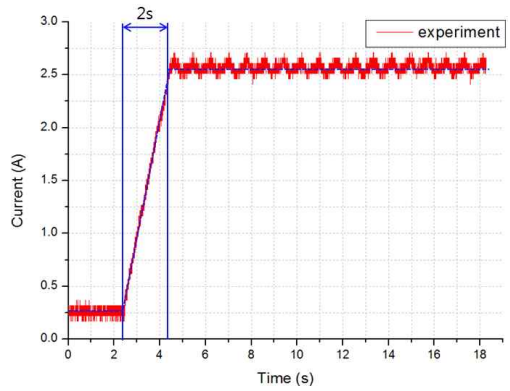

(b)

Fig. 12. 2s ramp recommand current results of double excited 3-DOF motor: (a) simulation (b) experiment.

5. Conclusion

This paper presented a dynamic analysis simulation system after the modeling of a 3-DOF machine using a nonlinear equivalent magnetic circuit and the electrical and mechanical systems. The simulation results were compared with the experimental results, and verified the accuracy and feasibility of the simulation system. Also, in the calculation time, we can say that these analysis method is very useful better than 3 dimensional numerical analysis for 3-DOF machine.

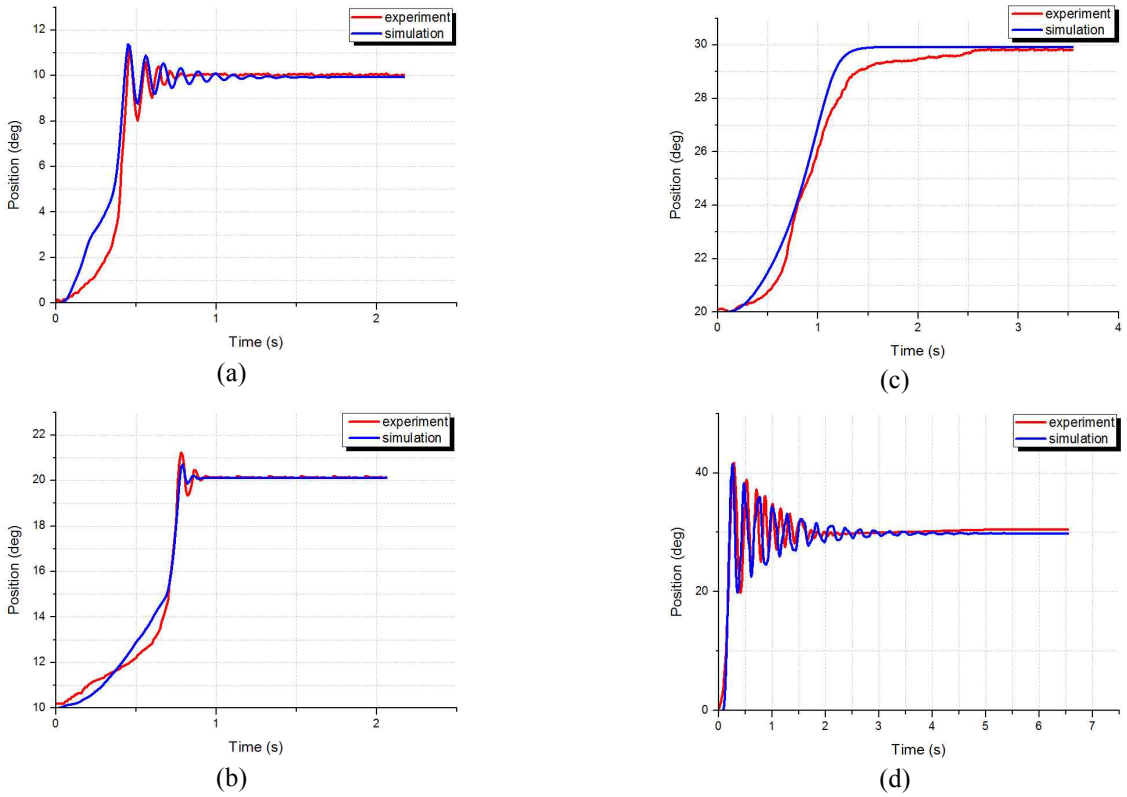

Fig. 13. Position results of double excited 3-DOF motor: (a) Rolling 1step, (b) Rolling 2step, (c) Rolling 3step, (d) Yawing 1step.

Acknowledgements

This research was supported by BK21PLUS program through the National Research Foundation of Korea funded by the Ministry of Education.

References

[1] Y. Hyun-Jong Park, Ho-Joon Lee, Su-YeonCho, Han-Woong Ahn, Ki-DoekLee, Chan-Yeop Park, Sung-Hong Won, and Ju Lee "A Performance Study on a Permanent Magnet Spherical Motor", IEEE Transactions on Magnetics, Vol. 49, no. 5, pp. 2307-2310, May 2013.

[2] M. Tsukano, Y. Sakaidani, K. Hirata, N. Niguchi, S. Maeda, and A. Zaini, "Analysis of 2-Degree of Freedom Outer Rotor Spherical Actuator Employing 3-D Finite Element Method", IEEE Transactions on Magnetics, Vol. 49, no. 5, pp. 2233-2236, May 2013.

[3] L.Yan, I. Chen, C. K. Lim, G.Yang, and K. M. Lee, "Modeling and Iron-Effect Analysis on Magnetic Field and Torque Output of Electromagnetic Spherical Actuators With Iron Stator", IEEE Transactions on Mechatronics, Vol.17, no.6, pp.1080-1087, Dec. 2012.

[4] Hyun-Jong Park, Su-Yoen Cho, Han-Woong Ahn, Ho-Jun Lee, Sung-Honh Won and Ju-Lee. "A Study of Advanced Spherical Motor for Improvement of Multi-DOF Motion." Journal of Electrical Engineering & Technology 7.6 (2012): 926-931.

[5] Ho-Joon Lee, Hyun-Jong Park, Sung-Hong Won, Gwang-Hyun Ryu and Ju Lee. "Improvements of Performance of Multi-DOF Spherical Motor by Double Air-gap Feature." Journal of Electrical Engineering & Technology 8.1 (2013): 90-96.

[6] Jae-sung Lee, Dae-kyung Kim, Soo-whang Baek, Se-hyun Rhyu, Byung-il Kwon, "Newly Structured Double Excited Two-Degree-of-Freedom Motor for Security Camera", IEEE Transactions on industry applications, Vol. 44, No. 11, pp. 4041-4044, Nov. 2008.

[7] B. I. Kwon, Y. B. Kim, "Design and Analysis of Double Excited 3-Degree-of-Freedom Motor for Robots", Journal of Electrical Engineering & Technology, Vol. 6, no. 5, pp. 618-625, 2011.

[8] H. U. Shin, M. Modarres, and B. I. Kwon, "Characteristic Analysis of Double Excited 3-DOF Motor by using Nonlinear Equivalent Magnetic Circuit", Industrial Electronics Society, IECON 2013 - 39th Annual Conference of the IEEE, pp. 2662-2667, 2013.

[9] J.T. Chen, Z.Q. Zhu, "Influence of the Rotr Pole Number on Optimal Parameters in Flux-Switching PM Brushless AC Machines by the Lumped-Parameter Magnetic Circuit Model", IEEE Transactions on industry applications, Vol. 46, No. 4, pp. 1381-

1388, Jul. 2010.
[10] Yoshiaki Kano, Takashi Kosaka, Nobuyuki Matsui, "Simple Nonlinear Magnetic Analysis for Permanent-Magnet Motors", IEEE Transactions on industry applications, Vol. 41, No. 5, pp. 1205-1214, Sep./ Oct. 2005.
[11] S. Maeda, N. Niguchi, "Dynamic Analysis of an Independently Controllable Electromagnetic Spherical Actuator", IEEE Transactions on Magnetics, Vol. 49, no. 5, May 2013.

Se-Hyun Rhyu He received the B.S., M.S., and Ph. D. degrees in electrical engineering from Hanyang University in 1996, 1998, and 2006, respectively. He has been the Korea Electronics Technology Institute currently since 1999. And he works also as a part-time professor at Hanyang University since 2009. His research activities are in the areas on Energy conversion systems which include the precision motor design and the optimized electrical machine of energy saving in industrial fields.

Byung-Il Kwon He received his B.S. and M.S. degrees in Electrical Engineering from Hanyang University, Korea and his Ph.D. in Electrical Engineering from Tokyo University, Japan. He is currently a Professor at Hanyang University. His research interests are linear drive systems, numerical analysis of electric machines and motor control.

Hye-Ung Shin He received his M.S. degrees in Electronic Information System Engineering from Hanyang University, Korea. His research interests are electrical actuator.

Min-Soo Kim He received his B.S. degrees in Electronic Information System Engineering from Hanyang University, Korea in 2012. He is currently working toward Ph.D. degree at Hanyang University. His research interests are design and analysis of electric machines.